doi:10.1093/brain/awr223 Brain 2011: 134; 2912–2928 | 2912

BRAIN
A JOURNAL OF NEUROLOGY

Altered functional–structural coupling of large-scale brain networks in idiopathic generalized epilepsy

Zhiqiang Zhang,[1,*] Wei Liao,[2,*] Huafu Chen,[2] Dante Mantini,[3] Ju-Rong Ding,[2] Qiang Xu,[2] Zhengge Wang,[1] Cuiping Yuan,[1] Guanghui Chen,[4] Qing Jiao[1] and Guangming Lu[1]

1 Department of Medical Imaging, Jinling Hospital, Nanjing University School of Medicine, Nanjing 210002, PR China
2 Key Laboratory for NeuroInformation of Ministry of Education, School of Life Science and Technology, University of Electronic Science and Technology of China, Chengdu 610054, PR China
3 Laboratory of Neuro-psychophysiology, K. U. Leuven Medical School, Leuven 3000, Belgium
4 Department of Neurology, Jinling Hospital, Nanjing University School of Medicine, Nanjing 210002, PR China

*These authors contributed equally to this work.

Correspondence to: Huafu Chen,
Key Laboratory for NeuroInformation of Ministry of Education,
School of Life Science and Technology,
University of Electronic Science and Technology of China,
Chengdu 610054,
PR China
E-mail: chenhf@uestc.edu.cn

Correspondence may also be addressed to: Guangming Lu, Department of Medical Imaging, Nanjing Jinling Hospital, 305#, Eastern Zhongshan Rd., Nanjing 210002, PR China. E-mail: cjr.luguangming@vip.163.com

The human brain is a large-scale integrated network in the functional and structural domain. Graph theoretical analysis provides a novel framework for analysing such complex networks. While previous neuroimaging studies have uncovered abnormalities in several specific brain networks in patients with idiopathic generalized epilepsy characterized by tonic–clonic seizures, little is known about changes in whole-brain functional and structural connectivity networks. Regarding functional and structural connectivity, networks are intimately related and share common small-world topological features. We predict that patients with idiopathic generalized epilepsy would exhibit a decoupling between functional and structural networks. In this study, 26 patients with idiopathic generalized epilepsy characterized by tonic–clonic seizures and 26 age- and sex-matched healthy controls were recruited. Resting-state functional magnetic resonance imaging signal correlations and diffusion tensor image tractography were used to generate functional and structural connectivity networks. Graph theoretical analysis revealed that the patients lost optimal topological organization in both functional and structural connectivity networks. Moreover, the patients showed significant increases in nodal topological characteristics in several cortical and subcortical regions, including mesial frontal cortex, putamen, thalamus and amygdala relative to controls, supporting the hypothesis that regions playing important roles in the pathogenesis of epilepsy may display abnormal hub properties in network analysis. Relative to controls, patients showed further decreases in nodal topological characteristics in areas of the default mode network, such as the posterior cingulate gyrus and inferior temporal gyrus. Most importantly, the degree of coupling between functional and structural connectivity networks was decreased, and exhibited a negative correlation with epilepsy duration in patients. Our findings suggest that the decoupling of

Received April 22, 2011. Revised July 11, 2011. Accepted August 1, 2011

functional and structural connectivity may reflect the progress of long-term impairment in idiopathic generalized epilepsy, and may be used as a potential biomarker to detect subtle brain abnormalities in epilepsy. Overall, our results demonstrate for the first time that idiopathic generalized epilepsy is reflected in a disrupted topological organization in large-scale brain functional and structural networks, thus providing valuable information for better understanding the pathophysiological mechanisms of generalized tonic–clonic seizures.

Keywords: idiopathic generalized epilepsy; generalized tonic–clonic seizures; structural connectivity network; functional connectivity network; coupling

Abbreviations: AAL = automated anatomical labelling; GTCS = generalized tonic–clonic seizures; IGE = idiopathic generalized epilepsy

Introduction

The human brain is a large-scale complex network, simultaneously segregated and integrated via specific connectivity patterns (Tononi *et al.*, 1994; Bullmore and Sporns, 2009; He and Evans, 2010; van den Heuvel and Hulshoff Pol, 2010). A quantitative analysis of complex brain networks, largely based on graph theory (Sporns, 2010; Bullmore and Bassett, 2011), is typically conducted through either the structural or functional domain (Damoiseaux and Greicius, 2009; Guye *et al.*, 2010). Structural connectivity networks can be based on white matter tracts quantified by diffusion tractography (Hagmann *et al.*, 2008; Iturria-Medina *et al.*, 2008; Gong *et al.*, 2009*a*) or correlations of morphological measures (He *et al.*, 2007; Zielinski *et al.*, 2010; Bernhardt *et al.*, 2011); they give insight into structural architectural features. Functional connectivity networks, on the other hand, can be calculated via temporal correlations or coherences between blood oxygen level-dependent functional MRI signals from distinct brain regions (Salvador *et al.*, 2005; Achard *et al.*, 2006); these functional connectivity networks offer a network perspective on brain dynamics. It has been suggested that the human network is organized to optimize efficiency, due to a small-world topology allowing simultaneous global and local parallel information processing (Bassett and Bullmore, 2006; Kaiser and Hilgetag, 2006). Indeed, a small-world architecture has been shown for functional connectivity networks (Salvador *et al.*, 2005; Achard *et al.*, 2006) and structural connectivity networks (Hagmann *et al.*, 2008; Iturria-Medina *et al.*, 2008; Gong *et al.*, 2009*a*).

The analysis of functional and structural connectivity networks provides new avenues for assessing complex network properties of the healthy and diseased brain (Damoiseaux and Greicius, 2009; Guye *et al.*, 2010). Indeed, an altered brain network topology has been shown in several psychiatric and neurological diseases, such as Alzheimer's disease (Lo *et al.*, 2010), schizophrenia (Liu *et al.*, 2008; van den Heuvel *et al.*, 2010; Zalesky *et al.*, 2011), stroke (Wang *et al.*, 2010), multiple sclerosis (Shu *et al.*, 2011) and temporal lobe epilepsy (Liao *et al.*, 2010; Bernhardt *et al.*, 2011). Furthermore, the simultaneous assessment of functional and structural connectivity networks allows for studying their relationship (Sporns, 2011). It has been suggested that the structural connectivity network may be the physical substrate of the functional connectivity network (van den Heuvel *et al.*, 2008; Greicius *et al.*, 2009). Several studies have demonstrated that structural connections are highly predictive of and place constraints on functional interactions across human brain networks (Koch *et al.*, 2002; Hagmann *et al.*, 2008; Greicius *et al.*, 2009; Honey *et al.*, 2009). Moreover, previous studies have documented large spatial resemblances between these two connectivity modalities within the whole-brain large-scale network (Honey *et al.*, 2009, 2010; van den Heuvel *et al.*, 2009*a*). Lastly, the coupling of functional and structural connectivity networks has been found to increase with age (Hagmann *et al.*, 2010; Supekar *et al.*, 2010) and to be disrupted in disease-specific states (Skudlarski *et al.*, 2010). Accordingly, the integration of functional and structural information from functional and structural connectivity networks may allow for the more sensitive detection of subtle brain pathophysiological abnormalities than any single modality.

Idiopathic generalized epilepsy (IGE) is a group of epileptic disorders characterized by widespread generalized spike-and-waves or polyspike–waves (Engel, 2001). Generalized tonic–clonic seizure (GTCS) is the most common phenotype of IGE (ILAE, 1989; Andermann and Berkovic, 2001), and is the type that requires the most medical attention. The most dangerous seizure symptoms of IGE-GTCS, including muscle rigidity, violent muscle contractions of entire body and complete loss of consciousness possibly cause injury or death. Undetectable focal anatomical brain lesion on routine MRI, high myoelectric contamination on ictal scalp EEG and the limited number of surgical cases make the understanding of IGE-GTCS challenging.

Although the conventional viewpoint for IGE-GTCS is that the entire brain may be homogeneously involved (Blumenfeld and Taylor, 2003), evidence from several imaging modalities specifically indicates that this form of epilepsy affects widespread brain through specific thalamocortical and corticocortical networks (Blumenfeld and Taylor, 2003; Blumenfeld *et al.*, 2003; Aghakhani *et al.*, 2004; Blumenfeld, 2005; Gotman *et al.*, 2005; Moeller *et al.*, 2008; Bernhardt *et al.*, 2009; Cavanna and Monaco, 2009). Recent network analyses have revealed that several distributed brain networks are involved in the genesis and manifestation of IGE (Li *et al.*, 2010; Luo *et al.*, 2011*a*, *b*; Wang *et al.*, 2011). As the global feature of the pathophysiology that widespread brain regions and extensive networks are involved in IGE-GTCS (Betting *et al.*, 2010), complex brain network investigation based on graph theory might be more valuable than local

connectional investigations to understand the mechanism of IGE-GTCS. In the present study, we tested three specific hypotheses:

(i) Network analyses in epilepsies other than IGE-CTCS have demonstrated alterations of brain network topology (Ponten *et al.*, 2009; van Dellen *et al.*, 2009; Chavez *et al.*, 2010; Horstmann *et al.*, 2010; Liao *et al.*, 2010; Bernhardt *et al.*, 2011). Ictal electrophysiology investigations have generally shown a more regular network organization after hyper-synchronous epileptic activities (Ponten *et al.*, 2007, 2009). Interictal studies, on the other hand, provided mixed findings. Electrophysiology and functional MRI studies have suggested a more random topology (Ponten *et al.*, 2007; van Dellen *et al.*, 2009; Liao *et al.*, 2010), but more regular topologies (Horstmann *et al.*, 2010) have also been observed in a recent network analysis of cortical thickness correlations (Bernhardt *et al.*, 2011). In this work, we will examine topological changes of interictal functional and structural connectivity networks in IGE-GTCS. As these changes might be associated with long-term impairments due to epilepsy duration (van Dellen *et al.*, 2009; Zhang *et al.*, 2009, 2010; Liao *et al.*, 2010; Vlooswijk *et al.*, 2010; Wang *et al.*, 2011), we will also test for such progressive effects in IGE-GTCS.

(ii) Previous findings in the functional (Gotman *et al.*, 2005; Song *et al.*, 2011; Wang *et al.*, 2011) and structural (Li *et al.*, 2010) domain suggest that IGE-GTCS relates to local abnormalities in several specific subcorticocortical networks (Blumenfeld, 2005, 2009). In this study, we wanted to employ measures of nodal topology, such as regional connectivity strength and efficiency, to characterize the role of individual regions for the functional integration of entire brain network (Rubinov and Sporns, 2010). We tested the hypothesis that the vital regions in the epileptic network, which are associated with generation, propagation and modulation of epileptic activity, will display abnormal hub property in network analysis (Frei *et al.*, 2010).

(iii) It is assumed that structural connectivity constrains functional connectivity, and that functional connectivity reversely exerts effect on structural connectivity through mechanisms of plasticity (Rubinov *et al.*, 2009; Hagmann *et al.*, 2010; Sporns, 2011). Regarding the reciprocal linkage between functional and structural connectivity, the functional and structural connectivity networks are intimately related and share common small-world topological features (Bullmore and Sporns, 2009; Honey *et al.*, 2009). In this work, we predict that the pathological state of IGE-GTCS may alter this network coupling, given that this type of epilepsy has widespread functional connectivity abnormalities (Moeller *et al.*, 2011; Song *et al.*, 2011; Wang *et al.*, 2011). Functional–structural connectivity coupling may provide a biomarker to detect subtle brain abnormalities more sensitively than any single modality, and may provide new insights into the understanding of the pathophysiological mechanisms of IGE-GTCS.

On the basis of the three aforementioned hypotheses to be tested, we combined state-of-the-art structural and functional connectivity network-based analyses, and investigated whole-brain network changes in patients with IGE-GTCS by comparing them with healthy subjects.

Materials and methods

Participants

The patient group was composed of 26 patients with IGE-GTCS [age (mean ± SD): 24.12 ± 6.85 years; age at first seizure onset: 18.15 ± 5.80 years; duration: 6.92 ± 5.80 years] recruited through Jinling Hospital, Nanjing University School of Medicine. These patients all met the following inclusion criteria: (i) presence of typical clinical symptoms of GTCS, including tic of limbs, loss of consciousness, no partial seizures; (ii) presence of generalized spike-and-wave or polyspike–waves discharges in their scalp EEG; (iii) no focal abnormality in routine structural MRI examinations; and (iv) no obvious history of aetiology. All patients were diagnosed as IGE with only GTCS according to the International League against Epilepsy (ILAE) classification. Fifteen patients were treated with anti-epileptic drugs, including valproate, phenytoin, carbamazepine, lamotrigine and topiramate (Supplementary Table 1).

Twenty-six age- and gender-matched healthy controls (age: 22.62 ± 2.06 years, all right-handed) were recruited from the staff of Jinling Hospital. Healthy controls were interviewed to confirm that there was no history of neurological disorder or psychiatric illness and no gross abnormalities in brain MRI images. There was no significant difference in age and gender between the two groups ($P > 0.05$).

Written informed consent was obtained from all participants. The study was approved by the local medical ethics committee at Jinling Hospital, Nanjing University School of Medicine.

Data acquisition

All patients during interictal state and healthy controls underwent structural, functional and diffusion tensor imaging scanning using a Siemens Trio 3T scanner at Jinling Hospital, Nanjing, China. Foam padding was used to minimize head motion for all subjects. Functional images were acquired using a single-shot, gradient-recalled echo planar imaging sequence (repetition time = 2000 ms, echo time = 30 ms and flip angle = 90°). Thirty transverse slices (field of view = 240 × 240 mm^2, in-plane matrix = 64 × 64, slice thickness = 4 mm, interslice gap = 0.4 mm, voxel size = 3.75 × 3.75 × 4 mm^3), aligned along the anterior commissure–posterior commissure line were acquired. For each subject, a total of 250 volumes were acquired, resulting in a total scan time of 500 s. Subjects were instructed simply to rest with their eyes closed, not to think of anything in particular, and not to fall asleep. The diffusion tensor images covering the whole brain were obtained using spin echo-based echo planar imaging sequence, including 30 volumes with diffusion gradients applied along 30 non-collinear directions (b = 1000 s/mm^2) and one volume without diffusion weighting (b = 0 s/mm^2). Each volume consisted of 45 contiguous axial slices (repetition time = 6100 ms, echo time = 93 ms, flip angle = 90°, field of view = 240 × 240 mm^2, matrix size = 256 × 256, voxel size = 0.94 × 0.94 × 3 mm^3). To improve the signal to noise ratio, the entire sequence was repeated four times. Subsequently, high-resolution T_1-weighted anatomical images were acquired in the sagittal orientation using a magnetization-prepared rapid

gradient-echo sequence (repetition time = 2300 ms, echo time = 2.98 ms, flip angle = 9°, field of view = 256 × 256 mm^2, matrix size = 256 × 256 and zero filled and interpolated to 512 × 512, slice thickness = 1 mm, without interslice gap, voxel size = 0.5 × 0.5 × 1 mm^3 and 176 slices) on each subject.

Brain network construction

Anatomical parcellation

To determine the nodes of brain functional and structural connectivity networks, we used the automated anatomical labelling (AAL) algorithm (Tzourio-Mazoyer *et al.*, 2002) to parcellate the whole cerebral cortex into 90 non-cerebellar anatomical regions of interest with low resolution (45 regions of interest for each hemisphere). This parcellation scheme is referred to as AAL-90. A list of anatomical labels of the nodes is presented in Supplementary Table 2. Considering that the range of nodal scales and the difference in template parcellations may result in considerable variation of graph theoretical parameters of functional connectivity networks (Wang *et al.*, 2009; Fornito *et al.*, 2010) and structural connectivity network (Zalesky *et al.*, 2010), we also used a high-resolution parcellation network with 1024 regions of interest to investigate brain functional and structural connectivity networks, as suggested previously (Fornito *et al.*, 2010; Zalesky *et al.*, 2010). To this end, we partitioned the 3D grey matter volume into *n* contiguous regions while constraining the size of nodes as uniformly as possible. Specifically, to generate a high-resolution nodal scale, each node composing the low-resolution native AAL template was subdivided into a set of micro-nodes. Each micro-node was constrained to lie within the volume encapsulated by its parent low-resolution AAL node and each micro-node was ensured to be contiguous. In turn, the native AAL segmentation was parcellated into 1024 micro regions of interest of approximately identical size (1.2 cm^3) across both hemispheres (512 regions of interest for each hemisphere). This parcellation scheme is referred to as AAL-1024 (Fornito *et al.*, 2010; Zalesky *et al.*, 2010) (Supplementary Fig. 1). These two types of parcellation schemes were applied in parallel to the following network analyses, for a cross-validation of our results.

Functional connectivity network construction

Functional images preprocessing was carried out using the Statistical Parametric Mapping software (SPM8, http://www.fil.ion.ucl.ac.uk/spm). Functional images, after exclusion of the first 10 images to ensure steady-state longitudinal magnetization, were initially corrected for temporal differences and head motion. No translation or rotation parameters in any given data set exceeded ±1 mm or ±1°, and no group differences were found in respect to head translation and rotation (both $P > 0.05$). Functional images were warped into a standard stereotaxic space at a 3 × 3 × 3 mm^3 resolution, using the Montreal Neurological Institute (MNI) echo-planar imaging template. In order to avoid introducing artificial local spatial correlations, no spatial smoothing was applied, as previously suggested (Salvador *et al.*, 2005; Achard *et al.*, 2006; Achard and Bullmore, 2007; Wang *et al.*, 2009). For each subject, representative time series in each region of interest were obtained by averaging the functional MRI time series across all voxels in the region of interest. To remove spurious sources of variance, time series were preprocessed as follows: first, six head motion parameters, averaged signals from CSF and white matter, and global brain signal were regressed (Fox *et al.*, 2005, 2009); next, the time series were band-pass filtered (0.01–0.08 Hz). We then obtained a temporal correlation matrix ($N \times N$, where $N = 90$ is the number of regions of interest in low-resolution AAL-90, and $N = 1024$ for high-resolution AAL-1024; whose elements are r_{ij}) for each subject by computing Pearson correlation coefficients between the processed time series of every pair of regions of interest. A weighted network can incorporate additional information on the strength of functional connections on continuous scales, enabling more comprehensive understanding network organizations. To construct weighted functional connectivity networks, weighted edges considered as absolute functional connectivity strength between connected regions of interest, e.g. $w_{ij} = |r_{ij}|$, where r_{ij} is the correlation coefficient for nodes *i* and *j*. For details about the construction of weighted functional connectivity network, see Supplementary Fig. 2.

Structural connectivity network construction

For each subject, diffusion-weighted images were geometrically corrected using a non-diffusion-weighted B0 image ($b = 0$ s/mm^2) and a field map, to account for eddy current distortions. Diffusion-weighted images were co-registered to the B0 image using affine transformations to minimize slight head movements. Diffusion tensor models were estimated by the linear least-squares fitting method at each voxel using the Diffusion Toolkit (trackvis.org; Wang *et al.*, 2007). Whole-brain fibre tracking was performed in native diffusion space for each subject using the Fibre Assignment by Continuous Tracking (FACT) algorithm embedded in the Diffusion Toolkit (Wang *et al.*, 2007). Path tracing proceeded until either the fractional anisotropy was <0.15 or the angle between the current and the previous path segment exceeded 35°, as in our previous study (Liao *et al.*, 2011). To determine the nodes of structural connectivity network in each subject, regions of interest were defined in native diffusion space (Gong *et al.*, 2009*a*; Li *et al.*, 2009). Accordingly, each individual structural image (i.e. T_1-weighted image) was first co-registered to their B0 images in the native diffusion space using a linear transformation. Co-registered structural images were then mapped to the ICBM-152 MNI T_1-template by applying an affine transformation with 12 degrees of freedom together with a series of non-linear warps characterized by a set of 7 × 8 × 7 basis functions. The derived transformation parameters were inverted and used to warp the AAL regions of interest from MNI space to the native diffusion space. This procedure has been applied in previous studies (Gong *et al.*, 2009*a*, *b*; Li *et al.*, 2009; Shu *et al.*, 2009; Lo *et al.*, 2010; Wen *et al.*, 2011). In native diffusion space, region of interest (*i*) and region of interest (*j*) were considered to be connected through an edge $e = (i, j)$, in case at least one fibre (*f*) were presented between them (Hagmann *et al.*, 2008, 2010; Gong *et al.*, 2009*a*). For each edge (*e*), we calculated the connection density (number of connection per unit surface) between the end-nodes as its weight $w(e)$ (Hagmann *et al.*, 2008, 2010; Honey *et al.*, 2009), according to $w(e) = 2/(S_i + S_j) \sum_{f \in F_e} 1/l(f)$.

In particular, S_i and S_j are 2D intersects of the individual's white matter (Liao *et al.*, 2011) with AAL region of interest (*i*) and region of interest (*j*), respectively; F_e denotes the set of all fibres connecting regions of interest *i* and *j* (hence contributing to the edge *e*); $l(f)$ denotes the length of the fibre *f* along its trajectory. By computing the weights across edges, we obtained a weighted structural connectivity network for each participant. For further details on weighted structural connectivity network construction, see Supplementary Fig. 3. Since there is currently no formal consensus regarding selection of indices for quantifying structural connectivity in tractography measurements, we also evaluated the effects of a variety of alternative entries in the weighted structural connectivity network, including fibre number related to the fibre quantity; mean fractional anisotropy values related to fibre integrity; and a combination of these measures (fibre number × fractional anisotropy) (Li *et al.*, 2009; Shu *et al.*, 2009; Lo *et al.*, 2010; Wen *et al.*, 2011) (Supplementary Fig. 4).

Network analysis

Graph theoretical analyses were carried out on functional and structural connectivity networks of patients with IGE-GTCS and healthy controls using the Brain Connectivity Toolbox (http://www.brain-connectivity-toolbox.net) (Rubinov and Sporns, 2010). For each individual structural connectivity network, connection weights were scaled by the maximum of this matrix to keep each subject's cost at the same level (Iturria-Medina *et al.*, 2008; van den Heuvel *et al.*, 2010).

Small-world properties

Small-world properties were originally proposed by Watts and Strogatz (1998). Here, we investigated small-world properties of weighted functional and structural connectivity networks (Achard and Bullmore, 2007; Lo *et al.*, 2010; Wen *et al.*, 2011; Yan *et al.*, 2011). The weighted clustering coefficient of a node i, C_i^w, which expresses the likelihood that the neighbourhoods of node i are connected (Onnela *et al.*, 2005), is defined as follows:

$$C_i^w = \frac{\sum_{j,h \in N} (w_{ij} w_{ih} w_{jh})^{1/3}}{k_i(k_i - 1)}$$

where w_{ij} is the weight between nodes i and j in the network, and k_i is the degree of node i. The clustering coefficient is zero, $C_i^w = 0$, if the nodes are isolated or with just one connection. The overall clustering coefficient, namely C_{net}^w, was computed as the average of C_i^w across all nodes in the network:

$$C_{net}^w = \frac{1}{N} \sum_{i \in N} C_i^w$$

extent measure of the local interconnectivity or cliquishness of the network (Watts and Strogatz, 1998).

The path length between nodes i and j was defined as the sum of the edge lengths along the path, where each edge's length was obtained by computing the reciprocal of the edge weight, $1/w_{ij}$. The shortest path length L_{ij} between nodes i and j and was defined as the length of the path with the shortest length between the two nodes. The weight characteristic shortest path length L_{net}^w of a network was measured by a 'harmonic mean' length between pairs (Newman, 2003), to overcome the problem of possibly disconnected network components. Formally, L_{net}^w is the reciprocal of the average of the reciprocals:

$$L_{net}^w = \frac{1}{1/(N(N-1)) \sum_{i=1}^{N} \sum_{j \neq i}^{N} 1/L_{ij}}$$

where N is the number of nodes. The weight characteristic shortest path length quantifies the ability for information propagation in parallel.

To examine small-world properties related to C_{net}^w and L_{net}^w, brain networks were compared to random networks. A small-world network has similar path length but higher clustering than a random network, that is $\gamma = C_{net}^w / C_{random}^w > 1$, $\lambda = L_{net}^w / L_{random}^w \approx 1$ (Watts and Strogatz, 1998). These two conditions can also be summarized into a scalar quantitative measurement, the small-worldness, $\sigma = \gamma/\lambda$, which is typically >1 in the case of small-world organization (Achard *et al.*, 2006; Humphries *et al.*, 2006). For each individual brain network, a set of 100 comparable random networks with similar degree sequence and symmetric adjacency matrix were formed, and C_{random}^w and L_{random}^w were defined as the average weighted clustering coefficient and weighted path length.

Nodal characteristics analysis

Three nodal topological characteristics, including nodal degree (S_i^w), efficiency (E_i^w) and betweenness centrality (b_i^w) were used. These measures are known to be interrelated, each provides a different viewpoint from which to discern major features of the large-scale architecture (Hagmann *et al.*, 2008; Tian *et al.*, 2011). The degree (S_i^w) was computed as the sum of the weights of all the connections of node i, that is $S_i^w = \sum_{j \in N} w_{ij}$.

The degree S_i^w quantifies the extent to which a node is relevant to the graph (Rubinov and Sporns, 2010). The total connection strength S_{net}^w of the network was computed as the sum of S_i^w for all nodes N in the network:

$$S_{net}^w = \frac{1}{N} \sum_{i \in N} S_i^w.$$

The nodal efficiency of a given node i(E_i^w) is defined as the inverse of the mean harmonic shortest path length between this node and all other nodes in the network (Achard and Bullmore, 2007; Shu *et al.*, 2011), according to the formula:

$$E_i^w = \frac{1}{N-1} \sum_{i \neq j \in N} \frac{1}{L_{ij}}$$

where L_{ij} is the weighted shortest path length between nodes i and j in the network. E_i^w quantifies the importance of the nodes for the communication within the network (Bassett and Bullmore, 2006). Accordingly, the node i is more important if the value of E_i^w is higher.

The betweenness centrality B_i^w of a node i considers the fraction of all shortest paths in the network that pass through the node (Freeman, 1977). In this study, we computed the normalized betweenness as $b_i^w = B_i^w / \langle B_i^w \rangle$, where $\langle B_i^w \rangle$ is the averaged nodal betweenness of the network. The global centrality measure b_i^w captures the influence of a node over information flow between other nodes in the network.

Nodes with high weighted degree, S_i^w can be considered as centres for information integration; those with high efficiency, E_i^w, are relevant for information flow; those with high betweenness centrality, b_i^w, may serve as way stations for network traffic. Accordingly, nodes with these properties were considered as network hubs. For each node, we calculated normalized nodal parameters as in the following formula (Tian *et al.*, 2011):

$$X_{norm}^w(i) = \frac{1/M \sum_{k=1}^{M} x_{nod}(i,k)}{1/(N \times M) \sum_{j=1}^{N} \sum_{k=1}^{M} x_{nod}(i,k)}$$

In this formula, $x_{nod}(i,k)$ is an integrated nodal parameter (weighted degree, efficiency and betweenness centrality) of node i in the network of subject k, M is the number of networks in the healthy controls ($M = 26$) and GTCS ($M = 26$) groups and N is the number of nodes ($N = 90$ and $N = 1024$ for AAL-90 and AAL-1024 parcellation schemes, respectively). Nodes with $X_{norm}(i) >$ mean + SD were considered as hubs in the brain network (He *et al.*, 2009; Bernhardt *et al.*, 2011; Tian *et al.*, 2011).

Coupling between functional and structural connectivity networks

For each subject, we quantified coupling between functional and structural connectivity networks. The correlation between functional and structural connectivity was constrained by the edges with

non-zeros structural connectivity. Specifically, the non-zero structural connectivity network edges within were extracted to produce a vector of structural connectivity values. Next, these values were resampled into a Gaussian distribution (Honey *et al.*, 2009; Hagmann *et al.*, 2010). The corresponding functional connectivity network edges were also extracted to form a vector of functional connectivity values. Subsequently, the Pearson's correlation between these two vectors was calculated to quantity the coupling between functional connectivity network and structural connectivity network. Moreover, we also calculated the probability densities for the functional connectivity values considering the constraint on structural connectivity (non-zeros edges) and for the remaining part (zeros edges).

Statistical analysis

We first compared overall graph characteristics of the functional and structural connectivity networks between the patients with IGE-GTCS and healthy controls. We selected a fixed cost to ensure that all functional and structural connectivity networks were fully connected and with a minimum number of spurious edges (Achard *et al.*, 2006; Achard and Bullmore, 2007; He *et al.*, 2007; Bernhardt *et al.*, 2011). The overall graph characteristics included the weighted connectivity strength (S^w_{net}), normalized weighted clustering coefficient (γ), normalized weighted characteristic shortest path length (λ) and small-world property (σ). Comparisons between IGE-GTCS and healthy controls were performed using permutation tests (Bassett *et al.*, 2008; van den Heuvel *et al.*, 2010). Accordingly, we computed actual between-group differences of the graph parameters (S^w_{net}, σ, γ and λ) of functional and structural connectivity networks. This difference was placed into a null permutation distribution of differences, calculated by randomly assigning each participant to one of the two groups with the same size as the original groups of IGE-GTCS and healthy controls. This procedure was repeated for 5000 permutations. We assigned a *P*-value to the between-group difference (IGE-GTCS versus healthy controls) by computing the proportion of differences exceeding the null distribution values. A threshold of $\alpha = 0.05$ was used for testing all graph characteristics. We applied this statistical procedure to network data from: (i) the AAL-90 scheme; cost = 0.18 for both the functional connectivity network and structural connectivity network. The following criteria were applied: all brain networks were fully connected, and the brain networks had a minimum number of spurious edges and distinguishable properties in comparison to degree-matched random networks (Achard *et al.*, 2006; Achard and Bullmore, 2007; He *et al.*, 2007; Liu *et al.*, 2008; Liao *et al.*, 2010; Bernhardt *et al.*, 2011); and (ii) the AAL-1024 scheme; cost = 0.0068, ensuring that the mean degree of the network was larger than the log of the number of nodes (He *et al.*, 2007).

As a previous study suggested that the network of each subject normally differs in both the number and weighting on the edges (Wen *et al.*, 2011), we applied a matching strategy prior to comparison between patients and healthy controls, in which the same network cost values ensured each graph having the same number of edges. Since there is currently no formal consensus regarding selection of thresholds, here we selected a range of cost threshold ($0.05 \leqslant$ cost $\leqslant 0.30$, step = 0.01) for functional and structural connectivity networks in the AAL-90 scheme. This approach is similar to comparisons performed by previous studies (He *et al.*, 2007; Bernhardt *et al.*, 2011).

Using the above permutation framework, we also compared the nodal properties (S^w_i, E^w_i and b^w_i) between the patients with IGE-GTCS and healthy controls. We used the false discovery rate to correct the multiple comparisons (Benjamini and Hochberg, 1995).

Finally, we compared the coupling of functional connectivity network–structural connectivity network between patients with IGE-GTCS and healthy controls by using permutation tests. Testing was performed on the difference of functional–structural connectivity coupling strength (i.e. the coefficient of correlation between functional connectivity and structural connectivity under constraint of non-zeros structural connectivity network edges).

Relationship between topological properties and clinical variables

To investigate the clinical relevance of altered brain network topologies in IGE-GTCS, we correlated the clinical variables, duration of epilepsy and seizure frequency, with the topological properties (S^w_{net}, γ, λ, σ, S^w_i, E^w_i and b^w_i) at a fixed cost (cost = 0.18 for both functional and structural connectivity networks). Moreover, these clinical variables were correlated to the strength of functional–structural connectivity network coupling. Pearson's correlation analysis was used, controlling for age as confounding variable ($P < 0.05$).

Reproducibility analysis

To test the reproducibility of our results, we carried out a split-half analysis (He et al., 2009; Shu et al., 2011). Specifically, we divided the healthy controls group into two subgroups, matched for age and gender (HC1: 13 participants, four females, age: 22.54 ± 2.14 years; HC2: 13 participants, five females, age: 22.69 ± 2.06 years). Similarly, we divided the GTCS group into two matched subgroups (IGE-GTCS1: 13 participants, five females, age: 24.08 ± 7.03 years; IGE-GTCS2: 13 participants, four females, age: 24.15 ± 6.96 years) (all $P > 0.43$). For each subgroup, both functional and structural connectivity networks were constructed and analysed analogously to the aforementioned whole-group analysis. To determine whether there was a consistent topological organization in the population (He et al., 2009), we computed Pearson's correlation coefficients for the correlation patterns of the both functional and structural connectivity networks between HC1 and HC2 subgroups and between IGE-GTCS1 and IGE-GTCS2 subgroups. We also compared the topological parameters (S^w_{net} and L^w_{net}) between each pair of subgroups using permutation testing.

Results

Overall topology of functional and structural connectivity networks

Both IGE-GTCS and healthy controls showed a small-world organization ($\sigma > 1$) in functional and structural connectivity networks constructed at all connection densities [$w(e)$], following either the low-resolution AAL-90 or high-resolution AAL-1024 parcellation schemes (Fig. 1 and Supplementary Fig. 5). However, significant differences between patients and healthy controls ($P < 0.05$) were found for specific network organization characteristics with the AAL-90 scheme, but not for the AAL-1024 scheme. With the former, functional and structural connectivity networks in patients with IGE-GTCS showed the similar patterns of network alterations: decrease in small-world topology (σ), decrease in normalized clustering coefficient (γ), but no change in normalized characteristic

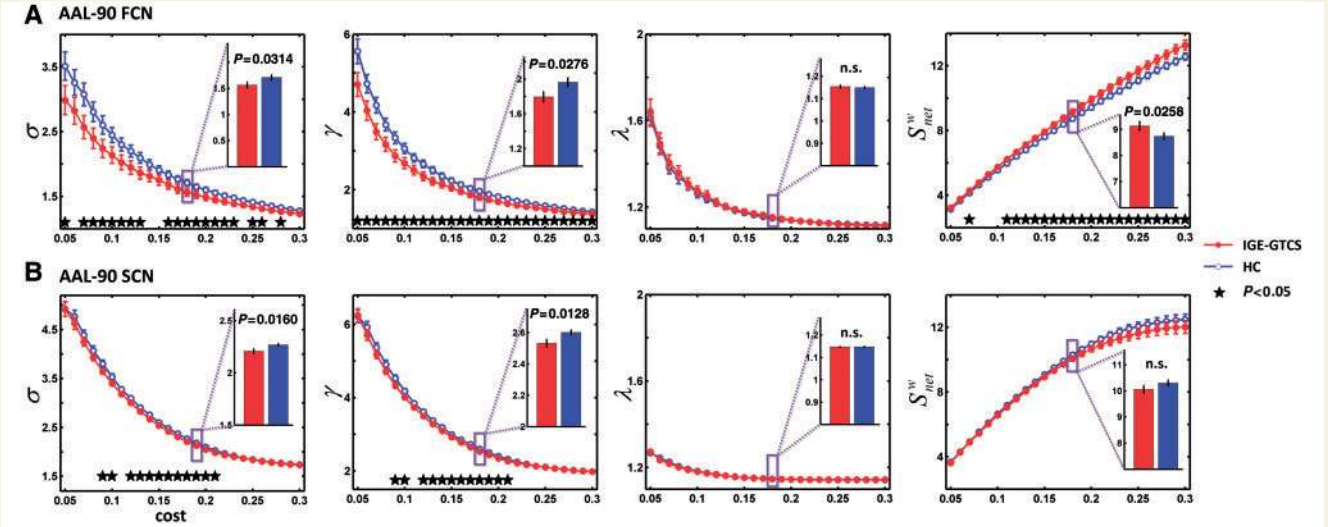

Figure 1 Overall characteristics of small-world topology (σ), normalized clustering coefficient (γ), normalized characteristic shortest path length (λ) and total connection strength (S^w_{net}) (left to right, respectively) of low-resolution AAL-90 functional connectivity network (**A**) and the structural connectivity network (**B**) as a function of cost thresholds. The stars indicate the significantly statistical difference between the IGE-GTCS and healthy controls groups (permutation testing, $P < 0.05$). The vertical bar indicates the standard deviation across subjects. The inset barplot indicates the statistical differences between groups at cost = 0.18 (permutation testing, $P < 0.05$). FCN = functional connectivity network; NS = no significance; SCN = structural connectivity network.

shortest path length (λ). While IGE-GTCS showed increased total connection strength (S^w_{net}) in the functional connectivity network, no change was found in the structural connectivity network (Fig. 1). Indices such as fractional anisotropy, fibre number and fractional anisotropy × fibre number also demonstrated small-world property, but no differences in small-worldness (σ) between patients with IGE-GTCS and healthy controls were found. Hence, the structural networks constructed by these indices were not analysed further. For overall topological indices of functional and structural connectivity networks, we found no correlation with duration of epilepsy and seizure frequency.

Nodal characteristics

Hub regions

We identified similar hub regions using the alternative characteristics weighted degree, efficiency and betweenness centrality. In line with the previous reports (Hagmann *et al.*, 2008; Gong *et al.*, 2009*b*; He *et al.*, 2009; Shu *et al.*, 2011; Tian *et al.*, 2011; Tomasi and Volkow, 2011; Yan *et al.*, 2011), we found that several nodes commonly presented network hub property across three measures (seven nodes including bilaterla insuli, left mesial orbital part of superior frontal gyrus, mesial superior frontal gyrus, supramarginal gyrus and middle frontal gyrus, and right post-central gyrus for the functional connectivity network; 10 nodes including the left middle frontal gyrus, paracentral lobule and orbital part of superior frontal gyrus, the right post-central gyrus, insular, orbital part of superior frontal gyrus, rectus gyrus, orbital part of middle frontal gyrus, calcarine fissure and middle occipital gyrus for the structural connectivity network). Moreover, there were convergent results between the AAL-90 (Supplementary Fig. 6) and AAL-1024 schemes (Supplementary Fig. 7).

Idiopathic generalized epilepsy-generalized tonic–clonic seizure-related alterations

Group comparisons on regional degree (S^w_i), efficiency (E^w_i), and betweenness centrality (b^w_i) revealed alterations of nodal characteristics in IGE-GTCS, with similar results for AAL-90 and AAL-1024 parcellation schemes (Fig. 2 and Supplementary Fig. 8).

In the functional connectivity network, increased S^w_i in IGE-GTCS were found in bilateral anterior cingulate gyrus, right amygdala, putamen, thalamus, left middle temporal gyrus and dorsolateral part of superior frontal gyrus; decreased S^w_i was found in left rolandic operculum, superior temporal pole and right inferior temporal gyrus (Fig. 2A). Differences in E^w_i in IGE-GTCS were similar to those seen in S^w_i. Increased E^w_i was found in bilateral anterior cingulate gyrus, left dorsolateral part of superior frontal gyrus, right putamen, amygdala and calcarine fissure; decreased E^w_i was found in left rolandic operculum, superior temporal pole, right inferior temporal gyrus and posterior cingulate gyrus (Fig. 2C). Increased b^w_i was found in left middle temporal gyrus and right amygdala; decreased b^w_i was found in right posterior cingulate gyrus. Both S^w_i ($r = 0.4275$, $P = 0.0293$) and E^w_i ($r = 0.4157$, $P = 0.0347$) of right amygdala positively correlated with epilepsy duration.

In the structural connectivity network, increased S^w_i in IGE-GTCS was found in left hippocampus; decreased S^w_i was found in bilateral anterior cingulate gyri, right pallidum and triangular part of inferior frontal gyrus (Fig. 2B). Increased E^w_i in IGE-GTCS was found in right olfactory cortex, fusiform gyrus and lingual gyrus; decreased E^w_i was found in bilateral anterior cingulate gyrus, right

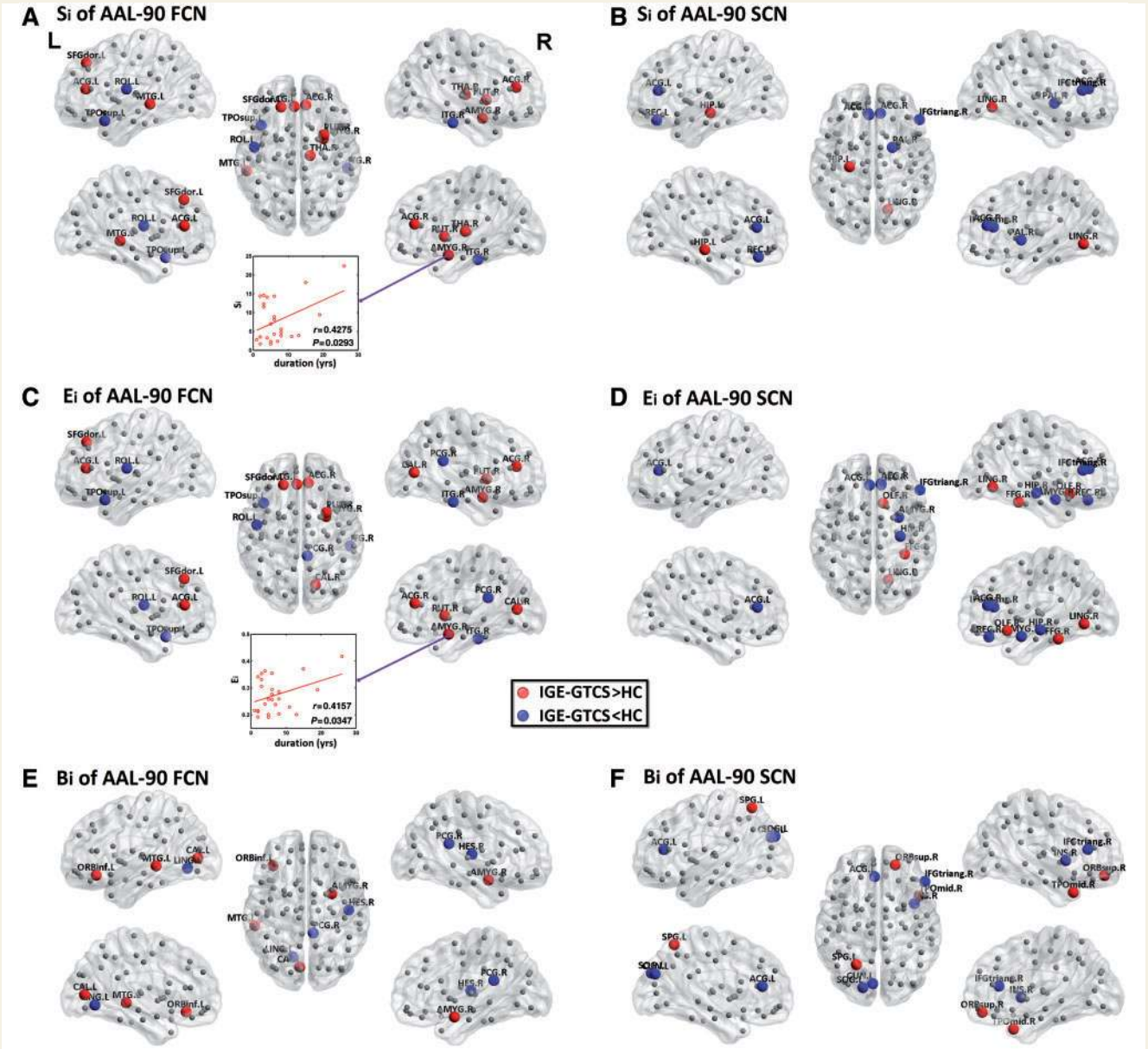

Figure 2 Alterations of S_i^w, E_i^w and b_i^w of functional and structural connectivity networks in patients with IGE-GTCS relative to healthy controls given a low-resolution AAL-90 parcellation scheme. Results were produced using permutation testing, and visualized using the BrainNet viewer (NKLCNL, Beijing Normal University). Three dimensional rendering maps show group differences of nodal degree (S_i^w) of the functional connectivity network (**A**) and structural connectivity network (**B**), group differences of nodal efficiency (E_i^w) of the functional connectivity network (**C**) and structural connectivity network (**D**); and betweenness centrality (b_i^w) of the functional connectivity network (**E**) and structural connectivity network (**F**). Red/blue spheres denote regions with increased/decreased nodal characteristic in patients. Grey dots denote regions with no difference between groups. Nodes were positioned according to their centroid stereotaxic coordinates. Scatter plots show the relationship between nodal characteristics and duration of epilepsy in IGE-GTCS. ACG = anterior cingulate gyrus; AMYG = amygdala; CAL = calcarine fissure; CUN = cuneus; FCN = functional connectivity network; FFG = fusiform gyrus; HES = Heschl gyrus; HIP = hippocampus; IFGtriang = triangular part of inferior frontal gyrus; INS = insula; ITG = inferior temporal gyrus; L = left; LING = lingual gyrus; MTG = middle temporal gyrus; OLF = olfactory cortex; ORBinf = oribital part of inferior frontal gyrus; ORBsup = orbital part of superior frontal gyrus; PAL = pallidum; PCG = posterior cingulate gyrus; PUT = putamen; REC = rectus gyrus; R = right; ROL = rolandic operculum; SFGdor = dorsolateral part of superior frontal gyrus; SOG = superior occipital gyrus; SPG = superior parietal gyrus; SCN = structural connectivity network; THA = thalamus; TPOmid = middle temporal gyrus, temporal pole; TPOsup = superior temporal gyrus, temporal pole.

triangular part of inferior frontal gyrus, amygdala, hippocampus, and rectus gyrus (Fig. 2D). The nodes in bilateral anterior cingulate gyrus showed a similar pattern of changes in S_i^w and E_i^w. Increased b_i^w was found in the right triangularis part of frontal gyrus pars triangularis; decreased b_i^w was found in the left anterior cingulate gyrus. In the structural connectivity network, no correlations between nodal characteristics and epilepsy variables were found.

Altogether, patterns of E_i^w alterations resembled those of S_i^w, but somewhat differed from those of b_i^w. Based on how frequently a region displayed significant group-differences across these three nodal measures, we identified the anatomical subregions as members of the core regions associated with IGE-GTCS alteration, including the regions showing alterations in at least two characteristics (Table 1) and one characteristic (Supplementary Table 3).

Altered functional–structural connectivity coupling

Similar to previous studies (Koch *et al.*, 2002; Hagmann *et al.*, 2008, 2010; Honey *et al.*, 2009), our results showed that not only the probability densities of functional connectivity values of structurally unconnected, but also that of structurally connected region pairs varied over a wide range (Supplementary Fig. 9). Under the constraint of existing structural connections, functional connectivity values positively correlated with structural connectivity values across all pairs of brain regions in each participant (Hagmann *et al.*, 2008, 2010; Honey *et al.*, 2009, 2010). This structural–functional connectivity statistical coupling was found for both AAL-90 and AAL-1024 parcellations (Fig. 3).

Compared with the healthy controls (0.2822 ± 0.0355 and 0.3412 ± 0.0279 for AAL-90 and AAL-1024 schemes), the patients with IGE-GTCS (0.1924 ± 0.0647 and 0.3190 ± 0.0386 for the AAL-90 and AAL-1024 schemes) showed a decrease in strength of functional–structural connectivity coupling ($P < 0.0001$ for AAL-90; $P = 0.0214$ for AAL-1024). Moreover, in patients, the strength of functional–structural connectivity coupling was negatively correlated with duration of epilepsy ($r = -0.4120$, $P = 0.0365$ for AAL-90; $r = -0.5954$, $P = 0.0013$ for AAL-1024) (Fig. 3).

Table 1 Summary of alterations of nodal characteristics in IGE-GTCS

Region	Modality	Strength	Efficiency	Betweenness
ACG.L	FCN	↑	↑	–
	SCN	↓	↓	↓
ACG.R	FCN	↑	↑	–
	SCN	↓	↓	–
SFGdor.L	FCN	↑	↑	–
	SCN	–	–	–
MTG.L	FCN	↑	–	↑
	SCN	–	–	–
PUT.R	FCN	↑	↑	–
	SCN	–	–	–
AMYG.R	FCN	↑	↑	↑
	SCN	–	↓	–
LING.R	FCN	–	–	–
	SCN	↑	↑	–
ROL.L	FCN	↓	↓	–
	SCN	–	–	–
TPOsup.L	FCN	↓	↓	–
	SCN	–	–	–
ITG.R	FCN	↓	↓	–
	SCN	–	–	–
PCG.R.	FCN	–	↓	↓
	SCN	–	–	–
IFGtriang.R	FCN	–	–	–
	SCN	↓	↓	↓

Upward arrow = region showing increase in the nodal topological characteristic in patients with IGE-GTCS. Downward arrow = region showing increase in the nodal topological characteristic. Dash = region showing no significant group difference of the nodal topological characteristic.

ACG = anterior cingulate gyrus; AMYG = amygdala; FCN = functional connectivity network; IFGtriang = triangular part of inferior frontal gyrus; ITG = inferior temporal gyrus; L = left; LING = lingual gyrus; MTG = middle temporal gyrus; PCG = posterior cingulate gyrus; PUT = putamen; R = right; ROL = rolandic operculum; SCN = structural connectivity network; SFGdor = superior frontal gyrus, dorsolateral part; TPOsup = superior temporal gyrus, temporal pole.

Reproducibility of findings

With either the AAL-90 or the AAL-1024 schemes, the previously constructed and matched split-half subgroups were similar in topological organization for both the functional connectivity network and the structural connectivity network. Visual inspection indicated similar connectivity patterns in these subgroups. Moreover, comparing the two healthy control subgroups (HC1 and HC2), we observed significant correlations in weight networks ($r = 0.9495$ and $r = 0.9659$ for AAL-90 functional and structural connectivity networks respectively; $r = 0.8795$ and $r = 0.9255$ for AAL-1024 functional and structural connectivity networks, respectively). A finding was also seen for the two IGE-GCTS subgroups ($r = 0.9401$ and $r = 0.9633$ for AAL-90 functional and structural connectivity networks, respectively; $r = 0.8787$ and $r = 0.9218$ for AAL-1024 functional and structural connectivity networks, respectively) (Fig. 4 and Supplementary Fig. 10). Comparisons of topological parameters were performed only for AAL-90. Neither comparison between the two healthy control subgroups (HC1 versus HC2, $P > 0.05$) nor comparison between the two IGE-GTCS subgroups (IGE-GTCS1 versus IGE-GTCS2, $P > 0.05$) showed significant differences in S_{net}^w and L_{net}^w. On the other hand, comparing patient with control groups, we observed significant differences in S_{net}^w (HC1 versus IGE-GTCS1, HC1 versus IGE-GTCS2, HC2 versus IGE-GTCS1 and HC2 versus IGE-GTCS2) and L_{net}^w (HC2 versus IGE-GTCS1) for the functional connectivity network (Fig. 4A). In addition, there were significant differences in the S_{net}^w (HC1 versus IGE-GTCS2 and HC2 versus IGE-GTCS1) and L_{net}^w (HC1 versus IGE-GTCS2, HC2 versus IGE-GTCS1 and HC2 versus IGE-GTCS2) for the structural connectivity network (Fig. 4B). These results suggest a high reproducibility of our findings.

Discussion

The present study applied for the first time graph theoretical analyses on both functional MRI and diffusion tensor imaging data to

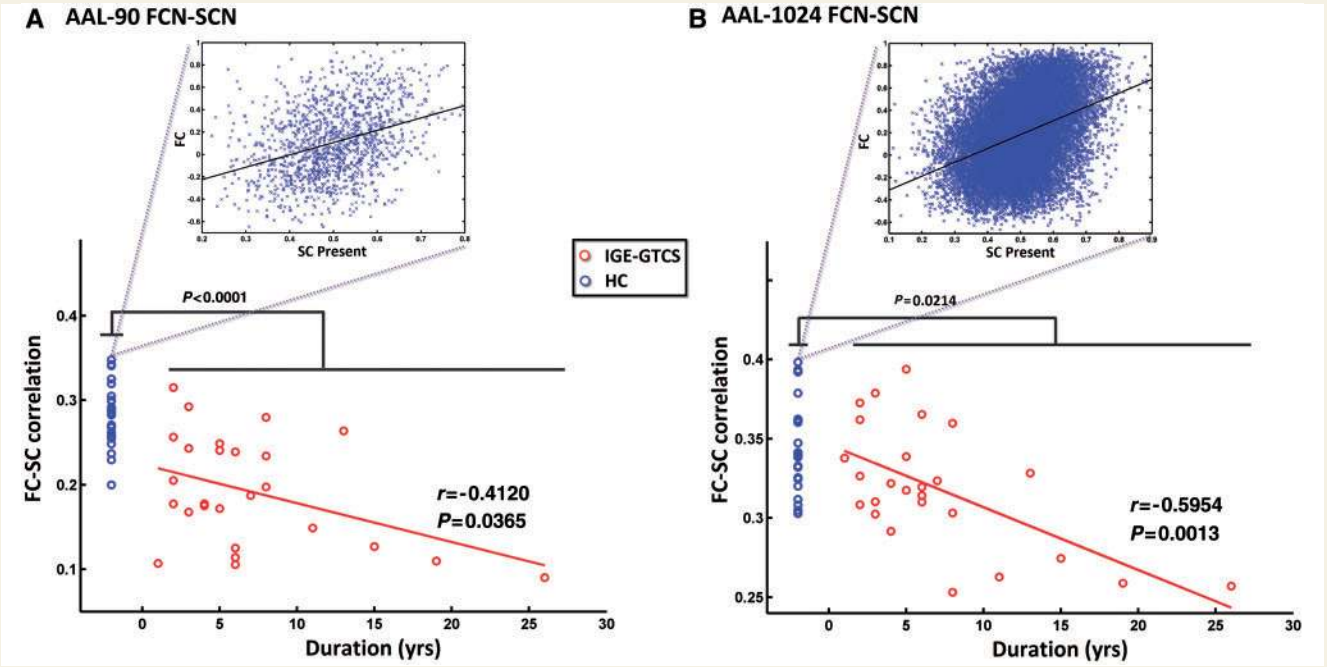

Figure 3 Disrupted functional–structural connectivity coupling in IGE-GTCS. Compared to healthy controls (HC), IGE-GTCS showed decreased functional–structural connectivity coupling (permutation testing, $P < 0.05$) in AAL-90 (**A**) and AAL-1024 (**B**). The strength of functional–structural connectivity coupling negatively correlated with duration of epilepsy in patients. The inset plots show the functional–structural connectivity coupling of selected individuals. FCN = functional connectivity network; SCN = structural connectivity network.

define and compare the functional and structural network topology in patients with IGE-GTCS. Our investigation revealed three main findings: (i) at the overall topological level, IGE-GTCS had altered small-worldness in both functional and structural connectivity networks, suggesting a more random organization in large-scale brain networks; (ii) at a nodal topological level, functional and structural connectivity networks showed altered nodal characteristics in cortical and subcortical regions previously shown to be involved in IGE-GTCS, such as the thalamus, anterior cingulate gyrus and default mode network regions (Gotman *et al.*, 2005; Luo *et al.*, 2011*b*; Song *et al.*, 2011); and (iii) the coupling of functional and structural connectivity networks was significantly decreased in IGE-GTCS, and this decrease was more marked in patients with a longer duration of epilepsy. The last finding may have clinical implications, as the index of coupling between functional and structural complex brain networks may be a potential biomarker for observation of epilepsy, and may provide new insights into the understanding of the pathophysiology of IGE-GTCS.

Altered overall topology of functional and structural connectivity networks

Consistent with the previous graph theoretical studies on epilepsy (Ponten *et al.*, 2007, 2009; Schindler *et al.*, 2008; van Dellen *et al.*, 2009; Horstmann *et al.*, 2010; Liao *et al.*, 2010; Bernhardt *et al.*, 2011), our results showed that both patients with IGE-GTCS and healthy controls have a small-world topology in functional and structural connectivity networks. Such a topology has been associated with simultaneous global and local parallel information processing (Bassett and Bullmore, 2006), and has been related to normal human cognitive functioning (van den Heuvel *et al.*, 2009*b*; Wen *et al.*, 2011) and the other pathological states (Liu *et al.*, 2008; Lo *et al.*, 2010; van den Heuvel *et al.*, 2010; Wang *et al.*, 2010; Shu *et al.*, 2011; Zalesky *et al.*, 2011), as presented with structural and functional brain networks. The present work contributed a novel case that patients with IGE-GTCS have an aberrant small-worldness, both in functional and structural connectivity networks (Fig. 1). These results suggest that patients with IGE-GTCS may have a less optimized network organization relevant to the specific pathological state than controls.

In patients with IGE-GTCS, both functional and structural connectivity networks showed significant decreases of normalized clustering coefficient (γ). γ is one of the key indices for checking the shifts of the network small-worldness to be more regular or random (He and Evans, 2010). The present results indicate a random shift of brain network architecture in IGE-GTCS. Concerning alterations of whole-brain network topology in patients with epilepsy, many studies using graph theoretical analysis of functional connectivity network have now been published, most of them using electrophysiological recordings (Ponten *et al.*, 2007, 2009; Kramer *et al.*, 2008, 2010; Schindler *et al.*, 2008). The periods of recording (interictal versus ictal) may contribute to the transitions of the network topological organizations. Commonly, functional network topology modifications during seizures show complex transitions but essentially a translation towards a more regular network in both partial and generalized epilepsy (Schindler *et al.*, 2008; Chavez *et al.*, 2010; Kramer *et al.*, 2010). A recent

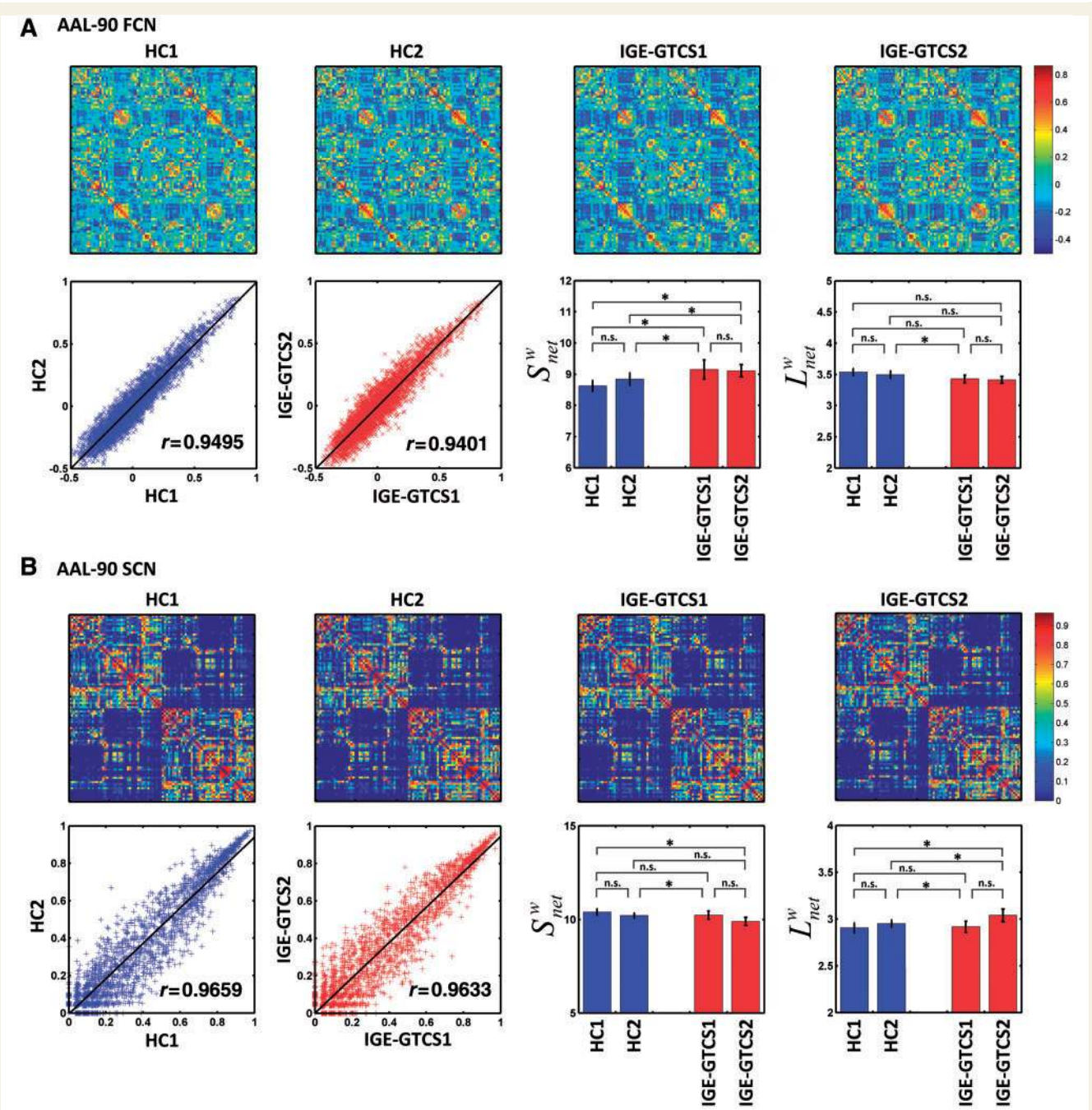

Figure 4 Evaluation of the reproducibility of the results for the functional connectivity network (**A**) and structural connectivity network (**B**). *Top*: mean network matrices of each subgroup (HC1, HC2, IGE-GTCS1 and IGE-GTCS2); the edge represents the connection weight between nodes. (*Bottom left*): the correlation between two healthy controls subgroups and between two IGE-GTCS subgroups. (*Bottom right*): significant differences in the two nodal characteristics between the two healthy controls subgroups and between the two IGE-GTCS subgroups. FCN = functional connectivity network; SCN = structural connectivity network.

interictal study using EEG and magnetoencephalography reported a more regular network in comparison with controls (Horstmann *et al.*, 2010). Moreover, a more regular topology has also been observed using structural networks constructed from cortical thickness correlations in a large sample of patients with drug-resistant temporal lobe epilepsy (Bernhardt *et al.*, 2011). Conversely, using resting-state functional MRI in relatively young patients with bilateral temporal lobe epilepsy, Liao and colleagues (2010) observed a more random topology during interictal periods. It may be possible that not only the epilepsy phenotype but also the modality of connectivity measurement partially accounts for some of those differences. Indeed, as the current results are based on functional MRI for the functional connectivity network and diffusion weighted imaging for the structural connectivity network,

they may not necessarily be comparable with data from electrophysiology for functional connectivity network and structural correlation analysis for structural connectivity network in the same cohort. Nevertheless, we detected consistent topological alterations in IGE-GTCS in both the functional and structural domain, thus possibly cross-validating our findings for these two modalities used.

In IGE-GTCS, the overall level of connectivity strength (S^w_{net}) was increased only in the functional connectivity network, but not in the structural connectivity network. S^w_{net} measures the global connectivity strength in the brain network (Hagmann *et al.*, 2008; Song *et al.*, 2011). An increased level of interictal functional connectivity in IGE-GTCS during resting-state is consistent with findings of several previous functional MRI studies (Luo *et al.*, 2011*a*, *b*; Wang *et al.*, 2011). It has been suggested that such increases may be associated with functional reorganization and plasticity (Song *et al.*, 2011; Wang *et al.*, 2011). In contrast to the finding of increased S^w_{net} in functional connectivity network, no change of S^w_{net} was found in structural connectivity network in patients with IGE-GTCS. Inconsistent topological characteristics between functional and structural connectivity networks have been reported previously (Park *et al.*, 2008). In general, the functional connectivity network is thought to be more flexible; while the structural connectivity network is relatively stable (Park *et al.*, 2008; Bullmore and Sporns, 2009). We therefore reasoned that the structural connectivity network may be less affected in patients with IGE-GTCS. In contrast, the functional connectivity network measured by blood oxygenation level-dependant fluctuations may be highly responsive to the perturbation of epileptic activity (Aghakhani *et al.*, 2004; Gotman *et al.*, 2005).

Altered nodal topology of functional and structural connectivity networks

Group comparisons of nodal topological characteristics revealed alterations of network hubs in IGE-GTCS, using a battery of alternative nodal measures. Patterns of nodal alterations were consistently using degree measures (S^w_i), nodal efficiency (E^w_i) and betweeness (b_{wi}). The characteristic of S^w_i is the most fundamental network measure, and provides information on the total degree of connectivity; E^w_i and b^w_i can both quantify the importance of the nodes for the communication within the network. These characteristics can be used to reflect the roles of nodes in information transport and integration across the network (Sporns *et al.*, 2007; Hagmann *et al.*, 2008; Song *et al.*, 2011). Given that these measures indicate similar abnormalities, abnormal hub architecture seems to be a consistent feature network disruption in IGE-GTCS.

Regions with increased hubness overlapped, in part, with regions previously shown to be involved in pathological subcortocortical networks of IGE (Archer *et al.*, 2003; Aghakhani *et al.*, 2004; Gotman *et al.*, 2005; Bernhardt *et al.*, 2009). The similar findings have previously been shown in temporal lobe epilepsy, where the authors also observed a higher proportion of paralimbic hubs in patients than in controls (Bernhardt *et al.*, 2011).

In the thalamus, we observed increases in S^w_i in the functional connectivity network. These findings likely underlie the central role of this structure in the generation, propagation and modulation of epileptic activity in IGE (Blumenfeld, 2003, 2005; Gotman *et al.*, 2005; Tyvaert *et al.*, 2009). Imaging evidence has also shown increased functional connectivity of the thalamocortical network in IGE (Blumenfeld, 2003, 2005). Our findings were consistent with the literature. Moreover, the findings might support the hypothesis that the epileptic focus may correspond to a strongly connected network node (Frei *et al.*, 2010).

We found the inferior temporal gyrus and temporal pole regions showed a decrease in E^w_i, and the posterior cingulate gyrus showed decreases in both E^w_i and b^w_i. These regions are known to be included in the default mode network (Raichle *et al.*, 2001; Fransson, 2005). Evidence from EEG-related functional MRI (Gotman *et al.*, 2005) and resting-state functional MRI studies (Luo *et al.*, 2011*a*; Song *et al.*, 2011; Wang *et al.*, 2011) has indicated that the abnormal default mode network function might underlie the pathophysiological mechanism of cognitive impairment in IGE. The present result repeated the functional abnormalities in the brain default mode regions in IGE-GTCS through the decreases in nodal topological properties.

In bilateral anterior cingulate gyrus relative to controls, we observed altered S^w_i and E^w_i in both the functional and structural connectivity networks. This region is considered as a predominant hub that may participate in multiple affective, cognitive and motor processes in the healthy brain (Achard and Bullmore, 2007; Seeley *et al.*, 2007; Buckner *et al.*, 2009; Tomasi and Volkow, 2011). In the pathophysiological process of IGE, mesial frontal regions and the anterior cingulate gyrus have also been shown to play important roles in the spreading and generalization of epileptic discharges and thalamocortical linkage (Isnard *et al.*, 2004; Gotman *et al.*, 2005; Stefan *et al.*, 2009).

Rather unexpectedly, we also observed that the amygdala presented increases in all three nodal topological characteristics in patients with IGE-GTCS. These alterations were furthermore shown to be positively correlated with duration of epilepsy in the characteristics of S^w_i and E^w_i. While the amygdala is consistently shown to be involved in temporal lobe epilepsy (Bonelli *et al.*, 2009; Mitsueda-Ono *et al.*, 2011), its role in IGE is less clear. On the other hand, being densely connected with both the thalamus and anterior cingulate gyrus, as shown by functional connectivity and diffusion tractography in humans (Behrens *et al.*, 2003; Di Martino *et al.*, 2008), the amygdala may participate in similar pathological processes as these two pathological hub regions during seizure generalization. Of note, amygdala kindling is an important technique in animal studies to elicit generalized seizures (McIntyre *et al.*, 1991). Another possibility is that the increased connections of amygdala might reflect emotional symptoms in IGE (Shehata and Bateh Ael, 2009). Future studies combining behavioural and neuroimaging data may be conducted to test these hypotheses.

Another unexpected finding was the asymmetry in the spatial distributions of altered nodes in IGE-GTCS. It is conventionally considered that the brain of IGE is bilaterally and symmetrically involved in IGE. Nonetheless, our findings are consistent with recent investigations, which have evidenced the asymmetric (Walser *et al.*, 2009) and lateralized (Casaubon *et al.*, 2003) features in IGE.

Interestingly, bilateral anterior cingulate gyrus and the right amygdala showed oppositely altered S_i^w and E_i^w between functional and structural connectivity networks. At present, this finding remains unclear. We can cautiously explain it on the basis of the difference in the underlying physiology between functional and structural connectivity. Enhanced functional connectivity may be related to a functional imbalance produced by epileptic activity (Luo *et al.*, 2011*a*, *b*; Wang *et al.*, 2011); conversely, a decrease in structural connectivity may be due to anatomical impairments related to the disease (Yogarajah *et al.*, 2008; Liao *et al.*, 2011). We believe that this opposed pattern of functional and structural connectivity network changes might mostly contribute to the functional–structural connectivity decoupling in the patients with IGE-GTCS.

Decoupling between functional and structural connectivity networks

In the present study, we combined functional MRI and diffusion tensor imaging techniques to investigate the structure–function relations in large-scale brain networks in patients with IGE-GTCS and healthy subjects. Functional network undergoes temporal coherence of blood oxygenation level-dependant fluctuations, and structural network takes advantage of water diffusion along myelinated nerve fibre tracts (Catani *et al.*, 2002; Johansen-Berg and Rushworth, 2009). Convergent functional and structural connectivity has been found in different levels varying from single cortical slice (Koch *et al.*, 2002) to resting-state networks (van den Heuvel *et al.*, 2008, 2009*a*; Greicius *et al.*, 2009) and even to large-scale whole-brain network (Hagmann *et al.*, 2008, 2010; Honey *et al.*, 2009). It is currently considered that structural connections are highly predictive of, and place constraint on, functional connection. Conversely, functional connections exert effects on structural connection through mechanisms of plasticity (Hagmann *et al.*, 2010). It has been previously observed that functional–structural connectivity coupling can be configured under physiological (Honey *et al.*, 2009; Hagmann *et al.*, 2010) or pathological states (Skudlarski *et al.*, 2010). This study for the first time concerns the function–structure relations in large-scale whole-brain networks in pathological state.

As we predicted, the network coupling between functional and structural connectivity was decreased in the patients with IGE-GTCS. The finding suggests that there is functional–structural connectivity decoupling in IGE-GTCS. The negative correlation between the coupling strengths and epilepsy durations further indicates that the functional–structural connectivity decoupling may be related to the progress of long-term impairment in patients. As aforementioned, no correlation was found between epilepsy durations and the overall characteristics of brain networks in any single imaging modality. Hence, we conclude that the index of functional–structural connectivity coupling has priority to capture the subtle changes of brain integration in IGE-GTCS. Of note, the causality between disturbed structural connectivity network architecture and cortical functional connectivity network dysfunction remains to be evaluated in future work.

Methodological considerations

Graph theoretical analysis of large-scale brain networks is a rapidly developing research field, but there are still some controversy concerning optimal analysis strategies (Bullmore and Bassett, 2011; Wig *et al.*, 2011). The current study employed several parallel data analysis approaches to provide a rich pool of information and furthermore cross-validate findings. Nevertheless, these findings also produced some inconsistent results. Such divergence might be driven by different node definitions by prior anatomic brain templates (Wang *et al.*, 2009) or node scales (Fornito *et al.*, 2010; Zalesky *et al.*, 2010). Secondly, we used four indices to construct the brain structural connectivity network, and we mainly discussed the results for the index of weight index connection density, $w(e)$, in line with the previous studies (Hagmann *et al.*, 2008, 2010; Honey *et al.*, 2009; Liao *et al.*, 2011; Yan *et al.*, 2011). This index combines fibre count and length between two nodes, and is likely to reflect the long-distance connections in complex neural systems (Hagmann *et al.*, 2008) better than other indices. Thirdly, such weighted networks contain information about connection strength that reflects heterogeneity in capacity and intensity of connections, and may thus be a more valid approach for brain network modelling. Moreover, it has been argued that using weighted networks is useful for reducing the influence of weak and potentially non-significant connections (Rubinov and Sporns, 2010). However, using weighted networks requires evaluating connectivity metrics at different thresholds, and thereby increases the problem complexity. Conversely, unweighted networks, having only binary edges, are simpler to use for statistical comparisons (Rubinov and Sporns, 2010). However, it does not directly reflect physical information related to the graph (Bullmore and Bassett, 2011). Fourthly, we used multiple cost thresholds ($0.05 \leqslant \text{cost} \leqslant 0.3$, step = 0.01) to evaluate the stability of the topological organization in networks calculated with low-resolution AAL-90 scheme. However, for comparing the overall and nodal characteristics between groups, we used a fixed cost (cost = 0.18 for both functional and structural connectivity networks with the AAL-90 scheme). Since multiple cost thresholds cannot be applied to structural connectivity networks constructed by deterministic tractography with the AAL-1024 structural connectivity network scheme, we used a fixed cost value (cost = 0.0068, the mean degree of the resulting network will being larger than the log of the number of node). Finally, we mainly used matched strategies to construct the structural connectivity network. The matched strategy meets the criterion that each network must have the same number of edges for brain network comparisons (Bullmore and Bassett, 2011). The unmatched strategy, for which all the edges are kept as long as there is a defined connection between two nodes, has also been used in the previous studies (Shu *et al.*, 2009, 2011; Lo *et al.*, 2010; Zalesky *et al.*, 2011). In this case, the numbers of edges of each individual network are potentially different from each other. We also explored the effect of different thresholds of fibre number on the structural connectivity network by using fibre number threshold values from 1 to 5. For each threshold value, the indices of S_{net}^w, C_{net}^w, σ, γ and λ were calculated. Group comparison analyses of these indices did not yield significant difference (Supplementary Table 4).

Limitations

Several limitations in the current study are noteworthy. First, our design does not allow us to control for confounding effects of anti-epileptic drugs, which can affect normal neuronal function and produce cognitive impairments (Ortinski and Meador, 2004). Secondly, we could not evaluate the potential effects on the brain networks of interictal epileptiform discharges since no simultaneous EEG data were acquired. Thirdly, previous studies have suggested that specific cognitive functions (Wen et al., 2011) and also general intellectual performance (Li et al., 2009; van den Heuvel et al., 2009b) are associated with brain network topological characteristics. Although we demonstrated alterations of network topologies in IGE-GTCS, the possible contribution to the behavioural and cognitive impairments in IGE-GTCS is still unclear, and requires future investigations. Finally, deterministic tractography was used to define the edges of the structural connectivity network according to other studies (Lo et al., 2010; Liao et al., 2011; Shu et al., 2011; Yan et al., 2011). The tracking procedure always stops when it reaches regions with fibre crossings (Mori and van Zijl, 2002), which might result in a loss of sensitivity. Probabilistic tractography techniques (Gong et al., 2009b) may be helpful to address the issue in future work.

Conclusion

In the present study, we combined the functional connectivity network (functional connectivity MRI) and the structural connectivity network (diffusion tractography) to investigate the alterations of the complex brain network organization in patients with IGE-GTCS. Although IGE-GTCS and healthy controls exhibited small-world topology in functional and structural connectivity networks, the patients showed reductions of the optimal topological organization in functional and structural connectivity networks. In addition, functional and structural connectivity networks showed altered nodal characteristics within a few key nodes associated with cortical and subcortical regions involved in IGE-GTCS. Importantly, we found deceased functional–structural connectivity network coupling in IGE-GTCS, and this decoupling was related to duration of the disorder, suggesting that the functional–structural connectivity network coupling may reflect the progress of IGE-GTCS. Overall, the present study demonstrates for the first time that the IGE-GTCS is associated with a disrupted topological organization in large-scale brain structural and functional network, opening up new avenues to better understanding this disorder.

Acknowledgements

We thank the patients and volunteers for participating in this study. We thank the anonymous reviewers for their constructive suggestions to improve this work. We thank Dr Yong He, Beijing Normal University, China, for his contribution to this work. We thank Andrew Zalesky, the University of Melbourne and Melbourne Health, Australia, for his providing code of high-resolution node parcellation and for his assistance. We also thank Ruopeng Wang, Van J. Wedeen, TrackVis.org, Martinos Center for Biomedical Imaging, Massachusetts General Hospital, for providing Diffusion Toolkit and TrackVis freely.

Funding

Natural Science Foundation of China (Grant nos. 30800264, 30971019, 90820006, 81020108022 and 61035006); Grants for Young Scholars in Jinling Hospital (Grant nos. Q2008063, 2011060); D.M. is a post-doc fellow of the Research Foundation Flanders (FWO) (Grant no. A4/5-SDS15387 to D.M.). Foundation of Changjiang Scholars and Innovative Research Team in University of Electronic science and technology of China.

Supplementary material

Supplementary material is available at *Brain* online.

References

Achard S, Bullmore E. Efficiency and cost of economical brain functional networks. PLoS Comput Biol 2007; 3: e17.

Achard S, Salvador R, Whitcher B, Suckling J, Bullmore E. A resilient, low-frequency, small-world human brain functional network with highly connected association cortical hubs. J Neurosci 2006; 26: 63–72.

Aghakhani Y, Bagshaw AP, Benar CG, Hawco C, Andermann F, Dubeau F, et al. fMRI activation during spike and wave discharges in idiopathic generalized epilepsy. Brain 2004; 127: 1127–44.

Andermann F, Berkovic SF. Idiopathic generalized epilepsy with generalized and other seizures in adolescence. Epilepsia 2001; 42: 317–20.

Archer JS, Abbott DF, Waites AB, Jackson GD. fMRI "deactivation" of the posterior cingulate during generalized spike and wave. Neuroimage 2003; 20: 1915–22.

Bassett DS, Bullmore E. Small-world brain networks. Neuroscientist 2006; 12: 512–23.

Bassett DS, Bullmore E, Verchinski BA, Mattay VS, Weinberger DR, Meyer-Lindenberg A. Hierarchical organization of human cortical networks in health and schizophrenia. J Neurosci 2008; 28: 9239–48.

Behrens TE, Johansen-Berg H, Woolrich MW, Smith SM, Wheeler-Kingshott CA, Boulby PA, et al. Non-invasive mapping of connections between human thalamus and cortex using diffusion imaging. Nat Neurosci 2003; 6: 750–7.

Benjamini Y, Hochberg Y. Controlling the false discovery rate—a practical and powerful approach to multiple testing. R Stat Soc Series B Stat Methodol 1995; 57: 289–300.

Bernhardt BC, Chen Z, He Y, Evans AC, Bernasconi N. Graph-Theoretical Analysis reveals disrupted small-world organization of cortical thickness correlation networks in temporal lobe epilepsy. Cereb Cortex 2011; 21: 2147–57.

Bernhardt BC, Rozen DA, Worsley KJ, Evans AC, Bernasconi N, Bernasconi A. Thalamo-cortical network pathology in idiopathic generalized epilepsy: insights from MRI-based morphometric correlation analysis. Neuroimage 2009; 46: 373–81.

Betting LE, Li LM, Lopes-Cendes I, Guerreiro MM, Guerreiro CA, Cendes F. Correlation between quantitative EEG and MRI in idiopathic generalized epilepsy. Hum Brain Mapp 2010; 31: 1327–38.

Blumenfeld H. From molecules to networks: cortical/subcortical interactions in the pathophysiology of idiopathic generalized epilepsy. Epilepsia 2003; 44 (Suppl 2): 7–15.

Blumenfeld H. Cellular and network mechanisms of spike-wave seizures. Epilepsia 2005; 46 (Suppl 9): 21–33.
Blumenfeld H, Taylor J. Why do seizures cause loss of consciousness? Neuroscientist 2003; 9: 301–10.
Blumenfeld H, Varghese GI, Purcaro MJ, Motelow JE, Enev M, McNally KA, et al. Cortical and subcortical networks in human secondarily generalized tonic-clonic seizures. Brain 2009; 132: 999–1012.
Blumenfeld H, Westerveld M, Ostroff RB, Vanderhill SD, Freeman J, Necochea A, et al. Selective frontal, parietal, and temporal networks in generalized seizures. Neuroimage 2003; 19: 1556–66.
Bonelli SB, Powell R, Yogarajah M, Thompson PJ, Symms MR, Koepp MJ, et al. Preoperative amygdala fMRI in temporal lobe epilepsy. Epilepsia 2009; 50: 217–27.
Buckner RL, Sepulcre J, Talukdar T, Krienen FM, Liu H, Hedden T, et al. Cortical hubs revealed by intrinsic functional connectivity: mapping, assessment of stability, and relation to Alzheimer's disease. J Neurosci 2009; 29: 1860–73.
Bullmore ET, Bassett DS. Brain graphs: graphical models of the human brain connectome. Annu Rev Clin Psychol 2011; 7: 113–40.
Bullmore E, Sporns O. Complex brain networks: graph theoretical analysis of structural and functional systems. Nat Rev Neurosci 2009; 10: 186–98.
Casaubon L, Pohlmann-Eden B, Khosravani H, Carlen PL, Wennberg R. Video-EEG evidence of lateralized clinical features in primary generalized epilepsy with tonic-clonic seizures. Epileptic Disord 2003; 5: 149–56.
Catani M, Howard RJ, Pajevic S, Jones DK. Virtual in vivo interactive dissection of white matter fasciculi in the human brain. Neuroimage 2002; 17: 77–94.
Cavanna AE, Monaco F. Brain mechanisms of altered conscious states during epileptic seizures. Nat Rev Neurol 2009; 5: 267–76.
Chavez M, Valencia M, Navarro V, Latora V, Martinerie J. Functional modularity of background activities in normal and epileptic brain networks. Phys Rev Lett 2010; 104: 118701.
Damoiseaux JS, Greicius MD. Greater than the sum of its parts: a review of studies combining structural connectivity and resting-state functional connectivity. Brain Struct Funct 2009; 213: 525–33.
Di Martino A, Scheres A, Margulies DS, Kelly AM, Uddin LQ, Shehzad Z, et al. Functional connectivity of human striatum: a resting state FMRI study. Cereb Cortex 2008; 18: 2735–47.
Engel J Jr. A proposed diagnostic scheme for people with epileptic seizures and with epilepsy: report of the ILAE task force on classification and terminology. Epilepsia 2001; 42: 796–803.
Fornito A, Zalesky A, Bullmore ET. Network scaling effects in graph analytic studies of human resting-state FMRI data. Front Syst Neurosci 2010; 4: 22.
Fox MD, Snyder AZ, Vincent JL, Corbetta M, Van Essen DC, Raichle ME. The human brain is intrinsically organized into dynamic, anticorrelated functional networks. Proc Natl Acad Sci USA 2005; 102: 9673–8.
Fox MD, Zhang D, Snyder AZ, Raichle ME. The global signal and observed anticorrelated resting state brain networks. J Neurophysiol 2009; 101: 3270–83.
Fransson P. Spontaneous low-frequency BOLD signal fluctuations: an fMRI investigation of the resting-state default mode of brain function hypothesis. Hum Brain Mapp 2005; 26: 15–29.
Freeman LC. A set of measures of centrality based upon betweenness. Sociometry 1977; 40: 35–41.
Frei MG, Zaveri HP, Arthurs S, Bergey GK, Jouny CC, Lehnertz K, et al. Controversies in epilepsy: debates held during the Fourth International Workshop on Seizure Prediction. Epilepsy Behav 2010; 19: 4–16.
Gong G, He Y, Concha L, Lebel C, Gross DW, Evans AC, et al. Mapping anatomical connectivity patterns of human cerebral cortex using in vivo diffusion tensor imaging tractography. Cereb Cortex 2009a; 19: 524–36.
Gong G, Rosa-Neto P, Carbonell F, Chen ZJ, He Y, Evans AC. Age- and gender-related differences in the cortical anatomical network. J Neurosci 2009b; 29: 15684–93.
Gotman J, Grova C, Bagshaw A, Kobayashi E, Aghakhani Y, Dubeau F. Generalized epileptic discharges show thalamocortical activation and suspension of the default state of the brain. Proc Natl Acad Sci USA 2005; 102: 15236–40.
Greicius MD, Supekar K, Menon V, Dougherty RF. Resting-state functional connectivity reflects structural connectivity in the default mode network. Cereb Cortex 2009; 19: 72–8.
Guye M, Bettus G, Bartolomei F, Cozzone PJ. Graph theoretical analysis of structural and functional connectivity MRI in normal and pathological brain networks. MAGMA 2010; 23: 409–21.
Hagmann P, Cammoun L, Gigandet X, Meuli R, Honey CJ, Wedeen VJ, et al. Mapping the structural core of human cerebral cortex. PLoS Biol 2008; 6: e159.
Hagmann P, Sporns O, Madan N, Cammoun L, Pienaar R, Wedeen VJ, et al. White matter maturation reshapes structural connectivity in the late developing human brain. Proc Natl Acad Sci USA 2010; 107: 19067–72.
He Y, Chen ZJ, Evans AC. Small-world anatomical networks in the human brain revealed by cortical thickness from MRI. Cereb Cortex 2007; 17: 2407–19.
He Y, Evans A. Graph theoretical modeling of brain connectivity. Curr Opin Neurol 2010; 23: 341–50.
He Y, Wang J, Wang L, Chen ZJ, Yan C, Yang H, et al. Uncovering intrinsic modular organization of spontaneous brain activity in humans. PLoS One 2009; 4: e5226.
Honey CJ, Sporns O, Cammoun L, Gigandet X, Thiran JP, Meuli R, et al. Predicting human resting-state functional connectivity from structural connectivity. Proc Natl Acad Sci USA 2009; 106: 2035–40.
Honey CJ, Thivierge JP, Sporns O. Can structure predict function in the human brain? Neuroimage 2010; 52: 766–76.
Horstmann MT, Bialonski S, Noennig N, Mai H, Prusseit J, Wellmer J, et al. State dependent properties of epileptic brain networks: comparative graph-theoretical analyses of simultaneously recorded EEG and MEG. Clin Neurophysiol 2010; 121: 172–85.
Humphries MD, Gurney K, Prescott TJ. The brainstem reticular formation is a small-world, not scale-free, network. Proc Biol Sci 2006; 273: 503–11.
ILAE. Proposal for revised classification of epilepsies and epileptic syndromes. Commission on Classification and Terminology of the International League Against Epilepsy. Epilepsia 1989; 30: 389–99.
Isnard J, Guenot M, Sindou M, Mauguiere F. Clinical manifestations of insular lobe seizures: a stereo-electroencephalographic study. Epilepsia 2004; 45: 1079–90.
Iturria-Medina Y, Sotero RC, Canales-Rodriguez EJ, Aleman-Gomez Y, Melie-Garcia L. Studying the human brain anatomical network via diffusion-weighted MRI and graph theory. Neuroimage 2008; 40: 1064–76.
Johansen-Berg H, Rushworth MF. Using diffusion imaging to study human connectional anatomy. Annu Rev Neurosci 2009; 32: 75–94.
Kaiser M, Hilgetag CC. Nonoptimal component placement, but short processing paths, due to long-distance projections in neural systems. PLoS Comput Biol 2006; 2: e95.
Koch MA, Norris DG, Hund-Georgiadis M. An investigation of functional and anatomical connectivity using magnetic resonance imaging. Neuroimage 2002; 16: 241–50.
Kramer MA, Eden UT, Kolaczyk ED, Zepeda R, Eskandar EN, Cash SS. Coalescence and fragmentation of cortical networks during focal seizures. J Neurosci 2010; 30: 10076–85.
Kramer MA, Kolaczyk ED, Kirsch HE. Emergent network topology at seizure onset in humans. Epilepsy Res 2008; 79: 173–86.
Li Y, Du H, Xie B, Wu N, Wang J, Wu G, et al. Cerebellum abnormalities in idiopathic generalized epilepsy with generalized tonic-clonic seizures revealed by diffusion tensor imaging. PLoS One 2010; 5: e15219.
Li Y, Liu Y, Li J, Qin W, Li K, Yu C, et al. Brain anatomical network and intelligence. PLoS Comput Biol 2009; 5: e1000395.
Liao W, Zhang Z, Pan Z, Mantini D, Ding J, Duan X, et al. Altered functional connectivity and small-world in mesial temporal lobe epilepsy. PLoS One 2010; 5: e8525.

Liao W, Zhang Z, Pan Z, Mantini D, Ding J, Duan X, et al. Default mode network abnormalities in mesial temporal lobe epilepsy: a study combining fMRI and DTI. Hum Brain Mapp 2011; 32: 883–95.

Liu Y, Liang M, Zhou Y, He Y, Hao Y, Song M, et al. Disrupted small-world networks in schizophrenia. Brain 2008; 131: 945–61.

Lo CY, Wang PN, Chou KH, Wang J, He Y, Lin CP. Diffusion tensor tractography reveals abnormal topological organization in structural cortical networks in Alzheimer's disease. J Neurosci 2010; 30: 16876–85.

Luo C, Li Q, Lai Y, Xia Y, Qin Y, Liao W, et al. Altered functional connectivity in default mode network in absence epilepsy: a resting-state fMRI study. Hum Brain Mapp 2011a; 32: 438–49.

Luo C, Li Q, Xia Y, Lei X, Xue K, Yao Z, et al. Resting state basal ganglia network in idiopathic generalized epilepsy. Human Brain Mapp 2011b, doi: 10.1002/hbm.21286.

McIntyre DC, Don JC, Edson N. Distribution of [14C]2-deoxyglucose after various forms and durations of status epilepticus induced by stimulation of a kindled amygdala focus in rats. Epilepsy Res 1991; 10: 119–33.

Mitsueda-Ono T, Ikeda A, Inouchi M, Takaya S, Matsumoto R, Hanakawa T, et al. Amygdalar enlargement in patients with temporal lobe epilepsy. J Neurol Neurosurg Psychiatry 2011; 82: 652–7.

Moeller F, Maneshi M, Pittau F, Gholipour T, Bellec P, Dubeau F, et al. Functional connectivity in patients with idiopathic generalized epilepsy. Epilepsia 2011; 52: 515–22.

Moeller F, Siebner HR, Wolff S, Muhle H, Boor R, Granert O, et al. Changes in activity of striato-thalamo-cortical network precede generalized spike wave discharges. Neuroimage 2008; 39: 1839–49.

Mori S, van Zijl PC. Fiber tracking: principles and strategies - a technical review. NMR Biomed 2002; 15: 468–80.

Newman MEJ. The structure and function of complex networks. SIAM Review 2003; 45: 167–256.

Onnela JP, Saramaki J, Kertesz J, Kaski K. Intensity and coherence of motifs in weighted complex networks. Phys Rev E Stat Nonlin Soft Matter Phys 2005; 71: 065103.

Ortinski P, Meador KJ. Cognitive side effects of antiepileptic drugs. Epilepsy Behav 2004; 5 (Suppl 1): S60–5.

Park C, Kim SY, Kim YH, Kim K. Comparison of the small-world topology between anatomical and functional connectivity in the human brain. Physica A: Stat Mech Appl 2008; 387: 5958–62.

Ponten SC, Bartolomei F, Stam CJ. Small-world networks and epilepsy: graph theoretical analysis of intracerebrally recorded mesial temporal lobe seizures. Clin Neurophysiol 2007; 118: 918–27.

Ponten SC, Douw L, Bartolomei F, Reijneveld JC, Stam CJ. Indications for network regularization during absence seizures: weighted and unweighted graph theoretical analyses. Exp Neurol 2009; 217: 197–204.

Raichle ME, MacLeod AM, Snyder AZ, Powers WJ, Gusnard DA, Shulman GL. A default mode of brain function. Proc Natl Acad Sci USA 2001; 98: 676–82.

Rubinov M, Sporns O. Complex network measures of brain connectivity: uses and interpretations. Neuroimage 2010; 52: 1059–69.

Rubinov M, Sporns O, van Leeuwen C, Breakspear M. Symbiotic relationship between brain structure and dynamics. BMC Neurosci 2009; 10: 55.

Salvador R, Suckling J, Coleman MR, Pickard JD, Menon D, Bullmore E. Neurophysiological architecture of functional magnetic resonance images of human brain. Cereb Cortex 2005; 15: 1332–42.

Schindler KA, Bialonski S, Horstmann MT, Elger CE, Lehnertz K. Evolving functional network properties and synchronizability during human epileptic seizures. Chaos 2008; 18: 033119.

Seeley WW, Menon V, Schatzberg AF, Keller J, Glover GH, Kenna H, et al. Dissociable intrinsic connectivity networks for salience processing and executive control. J Neurosci 2007; 27: 2349–56.

Shehata GA, Bateh Ael A. Cognitive function, mood, behavioral aspects, and personality traits of adult males with idiopathic epilepsy. Epilepsy Behav 2009; 14: 121–4.

Shu N, Liu Y, Li K, Duan Y, Wang J, Yu C, et al. Diffusion tensor tractography reveals disrupted topological efficiency in white matter structural networks in multiple sclerosis. Cereb Cortex 2011, doi:10.1093/cercor/bhr039.

Shu N, Liu Y, Li J, Li Y, Yu C, Jiang T. Altered anatomical network in early blindness revealed by diffusion tensor tractography. PLoS One 2009; 4: e7228.

Skudlarski P, Jagannathan K, Anderson K, Stevens MC, Calhoun VD, Skudlarska BA, et al. Brain connectivity is not only lower but different in schizophrenia: a combined anatomical and functional approach. Biol Psychiatry 2010; 68: 61–9.

Song M, Du H, Wu N, Hou B, Wu G, Wang J, et al. Impaired resting-state functional integrations within default mode network of generalized tonic-clonic seizures epilepsy. PLoS One 2011; 6: e17294.

Sporns O. Networks of the brain. Cambridge: MA: MIT Press; 2010.

Sporns O. The human connectome: a complex network. Ann N Y Acad Sci 2011; 1224: 109–25.

Sporns O, Honey CJ, Kotter R. Identification and classification of hubs in brain networks. PLoS One 2007; 2: e1049.

Stefan H, Paulini-Ruf A, Hopfengartner R, Rampp S. Network characteristics of idiopathic generalized epilepsies in combined MEG/EEG. Epilepsy Res 2009; 85: 187–98.

Supekar K, Uddin LQ, Prater K, Amin H, Greicius MD, Menon V. Development of functional and structural connectivity within the default mode network in young children. Neuroimage 2010; 52: 290–301.

Tian L, Wang J, Yan C, He Y. Hemisphere- and gender-related differences in small-world brain networks: a resting-state functional MRI study. Neuroimage 2011; 54: 191–202.

Tomasi D, Volkow ND. Association between functional connectivity hubs and brain networks. Cereb Cortex 2011; 21: 2003–13.

Tononi G, Sporns O, Edelman GM. A measure for brain complexity: relating functional segregation and integration in the nervous system. Proc Natl Acad Sci USA 1994; 91: 5033–7.

Tyvaert L, Chassagnon S, Sadikot A, LeVan P, Dubeau F, Gotman J. Thalamic nuclei activity in idiopathic generalized epilepsy: an EEG-fMRI study. Neurology 2009; 73: 2018–22.

Tzourio-Mazoyer N, Landeau B, Papathanassiou D, Crivello F, Etard O, Delcroix N, et al. Automated anatomical labeling of activations in SPM using a macroscopic anatomical parcellation of the MNI MRI single-subject brain. Neuroimage 2002; 15: 273–89.

van Dellen E, Douw L, Baayen JC, Heimans JJ, Ponten SC, Vandertop WP, et al. Long-term effects of temporal lobe epilepsy on local neural networks: a graph theoretical analysis of corticography recordings. PLoS One 2009; 4: e8081.

van den Heuvel MP, Hulshoff Pol HE. Exploring the brain network: a review on resting-state fMRI functional connectivity. Eur Neuropsychopharmacol 2010; 20: 519–34.

van den Heuvel MP, Mandl RC, Kahn RS, Hulshoff Pol HE. Functionally linked resting-state networks reflect the underlying structural connectivity architecture of the human brain. Hum Brain Mapp 2009a; 30: 3127–41.

van den Heuvel M, Mandl R, Luigjes J, Hulshoff Pol H. Microstructural organization of the cingulum tract and the level of default mode functional connectivity. J Neurosci 2008; 28: 10844–51.

van den Heuvel MP, Mandl RC, Stam CJ, Kahn RS, Hulshoff Pol HE. Aberrant frontal and temporal complex network structure in schizophrenia: a graph theoretical analysis. J Neurosci 2010; 30: 15915–26.

van den Heuvel MP, Stam CJ, Kahn RS, Hulshoff Pol HE. Efficiency of functional brain networks and intellectual performance. J Neurosci 2009b; 29: 7619–24.

Vlooswijk MC, Jansen JF, de Krom MC, Majoie HM, Hofman PA, Backes WH, et al. Functional MRI in chronic epilepsy: associations with cognitive impairment. Lancet Neurol 2010; 9: 1018–27.

Walser G, Unterberger I, Dobesberger J, Embacher N, Falkenstetter T, Larch J, et al. Asymmetric seizure termination in primary and secondary generalized tonic-clonic seizures. Epilepsia 2009; 50: 2035–9.

Wang R, Beener T, Sorensen AG, Weeden VJ. Diffusion toolkit: a software package for diffusion imaging data processing and tractography. Proc Intl Soc Mag Reson Med 2007; 3720.

Wang Z, Lu G, Zhang Z, Zhong Y, Jiao Q, Tan Q, et al. Altered resting state networks in epileptic patients with generalized tonic-clonic seizures. Brain Res 2011; 1374: 134–41.

Wang J, Wang L, Zang Y, Yang H, Tang H, Gong Q, et al. Parcellation-dependent small-world brain functional networks: a resting-state fMRI study. Hum Brain Mapp 2009; 30: 1511–23.

Wang L, Yu C, Chen H, Qin W, He Y, Fan F, et al. Dynamic functional reorganization of the motor execution network after stroke. Brain 2010; 133: 1224–38.

Watts DJ, Strogatz SH. Collective dynamics of 'small-world' networks. Nature 1998; 393: 440–2.

Wen W, Zhu W, He Y, Kochan NA, Reppermund S, Slavin MJ, et al. Discrete neuroanatomical networks are associated with specific cognitive abilities in old age. J Neurosci 2011; 31: 1204–12.

Wig GS, Schlaggar BL, Petersen SE. Concepts and principles in the analysis of brain networks. Ann N Y Acad Sci 2011; 1224: 126–46.

Yan C, Gong G, Wang J, Wang D, Liu D, Zhu C, et al. Sex- and brain size-related small-world structural cortical networks in young adults: a DTI tractography study. Cereb Cortex 2011; 21: 449–58.

Yogarajah M, Powell HW, Parker GJ, Alexander DC, Thompson PJ, Symms MR, et al. Tractography of the parahippocampal gyrus and material specific memory impairment in unilateral temporal lobe epilepsy. Neuroimage 2008; 40: 1755–64.

Zalesky A, Fornito A, Harding IH, Cocchi L, Yucel M, Pantelis C, et al. Whole-brain anatomical networks: does the choice of nodes matter? Neuroimage 2010; 50: 970–83.

Zalesky A, Fornito A, Seal ML, Cocchi L, Westin CF, Bullmore ET, et al. Disrupted axonal fiber connectivity in schizophrenia. Biol Psychiatry 2011; 69: 80–9.

Zhang Z, Lu G, Zhong Y, Tan Q, Liao W, Chen Z, et al. Impaired perceptual networks in temporal lobe epilepsy revealed by resting fMRI. J Neurol 2009; 256: 1705–13.

Zhang Z, Lu G, Zhong Y, Tan Q, Liao W, Wang Z, et al. Altered spontaneous neuronal activity of the default-mode network in mesial temporal lobe epilepsy. Brain Res 2010; 1323: 152–60.

Zielinski BA, Gennatas ED, Zhou J, Seeley WW. Network-level structural covariance in the developing brain. Proc Natl Acad Sci USA 2010; 107: 18191–6.